

Linearized flavor-stability analysis of dense neutrino streams

Arka Banerjee,¹ Amol Dighe,¹ and Georg Raffelt²

¹*Tata Institute of Fundamental Research, Homi Bhabha Road, Mumbai 400005, India*

²*Max-Planck-Institut für Physik (Werner-Heisenberg-Institut), Föhringer Ring 6, 80805 München, Germany*

(Dated: November 27, 2024)

Neutrino-neutrino interactions in dense neutrino streams, like those emitted by a core-collapse supernova, can lead to self-induced neutrino flavor conversions. While this is a nonlinear phenomenon, the onset of these conversions can be examined through a standard stability analysis of the linearized equations of motion. The problem is reduced to a linear eigenvalue equation that involves the neutrino density, energy spectrum, angular distribution, and matter density. In the single-angle case, we reproduce previous results and use them to identify two generic instabilities: The system is stable above a cutoff density (“cutoff mode”), or can approach an asymptotic instability for increasing density (“saturation mode”). We analyze multi-angle effects on these generic types of instabilities and find that even the saturation mode is suppressed at large densities. For both types of modes, a given multi-angle spectrum typically is unstable when the neutrino and electron densities are comparable, but stable when the neutrino density is much smaller or much larger than the electron density. The role of an instability in the SN context depends on the available growth time and on the range of affected modes. At large matter density, most modes are off-resonance even when the system is unstable.

PACS numbers: 14.60.Pq, 97.60.Bw

I. INTRODUCTION

Neutrino flavor oscillations in a supernova (SN) are strongly suppressed by matter effects [1] until the neutrinos pass through the usual MSW region [2–5] far out in the envelope of the collapsing star. However, neutrino-neutrino interactions [6, 7], through a flavor off-diagonal refractive index, can trigger self-induced flavor conversions [8–13]. This collective effect tends to occur between the neutrino sphere and the MSW region and can lead to strongly modified neutrino spectra, showing features such as spectral swaps and splits [14–19]; for a review see Ref. [20]. The overall scenario, supported by heuristic arguments and numerical examples, is that deep inside the SN core, the system performs “synchronized oscillations” with an extremely small amplitude, i.e. every neutrino remains essentially stuck in its initial flavor eigenstate. As the neutrinos stream outwards, there is a sharp onset radius where “bimodal” oscillations begin: Some ranges of modes start pendulum-like oscillations [11, 21–23], exchanging their flavor content with each other without affecting the flavor content of the overall system.

This scenario engenders a crucial simplification for the treatment of neutrino transport in SN simulations. At high densities, where neutrinos collide frequently, it is enough to solve the transport equations for each flavor separately, ignoring oscillations entirely. On the other hand, flavor conversions at larger distances can be treated ignoring neutrino collisions and absorption, i.e. as a pure propagation problem. So collisions and flavor oscillations are phenomena that are assumed to be taking place in different regions of the star and can be treated independently. When the radial distance where bimodal oscillations begin is far away from the SN core, this assumption is valid and the flavor conversions do not affect the SN

dynamics. Recent studies dedicated to the SN accretion phase, under simplifying assumptions, once more confirm this picture [24, 25].

However, what is missing is a systematic approach to decide, without solving the equations of motion, if self-induced flavor conversions occur for given neutrino spectra (flavor-dependent energy and angular distribution), overall neutrino density, and matter density. Formal stability criteria exist only in the “single-angle approximation” where it is assumed that all neutrinos feel the same neutrino-neutrino refractive effect. In this case the analytic pendulum solution has been found and its existence and parameters can be calculated from the neutrino spectrum and density alone [19].

On the other hand, the current-current nature of the low-energy weak-interaction Hamiltonian implies that neutrinos in the background of an anisotropic neutrino flux experience a refractive effect that strongly depends on direction. For some energy spectra, these “multi-angle effects” have little impact, whereas in other cases they completely change the solution. A SN neutrino flux with a vanishing net ν_e flux is unstable everywhere and shows quick multi-angle decoherence [26]. If the ν_e flux is large enough, this effect is avoided if the energy spectrum is simple [27]. More complicated spectra can be unstable even for a large ν_e flux at any density in the single-angle case, but the instability is suppressed by multi-angle effects [28, 29]. In addition, the presence of ordinary matter causes a multi-angle suppression of the bimodal instability [30]. On the other hand, it was claimed that for nontrivial angular distributions, as may exist when different flavors are emitted from very different neutrino spheres, there is a novel multi-angle instability [12]. Deviations from the usually assumed cylindrical symmetry may also have an important influence [13].

Although our problem is nonlinear and therefore would seem intractable, noting that an instability must occur in order for the onset to take place leads to a surprising simplification. In the dense SN matter well inside of the MSW region, the matter effect is so large that neutrino propagation eigenstates are essentially identical with flavor eigenstates. This means that in the weak-interaction basis, the flavor matrices of occupation numbers are almost perfectly diagonal, allowing us to linearize the equations of motion (EoMs) in terms of the small off-diagonal elements. An instability is equivalent to some of these small elements starting to grow exponentially. All we need to do is linearize the EoMs, perform a Fourier analysis, and seek exponentially growing solutions of the relevant eigenvalue equation. This is simple even in the multi-angle situation. Almost certainly this approach can be extended to cases without the usually assumed cylindrical symmetry around the radial direction.

Studying the stability of a strongly coupled and nonlinear system in the small-amplitude limit is a standard technique. In the present context it was put forth in Ref. [13]. However, the method was carried only to schematic cases of a small number of neutrino momentum modes, leaving open how to apply it to realistic situations.

While a stability analysis provides crucial insight, we stress that it alone is not enough to assess the impact in the SN context. Only a small range of modes may participate in the bimodal oscillation or the growth rate may be too small on the available time scale. (Of course, both the growth rate and the location of the resonance on the energy-angle spectrum are found by solving the eigenvalue equation.) For example, the classic single-angle case with an initial Fermi-Dirac spectrum of only ν_e and $\bar{\nu}_e$ is always unstable and the usual concept of a synchronization radius does not apply. However, for large neutrino densities, the growth rate is small and only a narrow range of infrared modes is affected. A “visible” effect arises only at a quasi-onset radius where the growth rate begins to compete with the overall evolution time scale and the resonance begins to move into the main part of the spectrum. We will here largely avoid such issues and concentrate on setting up the method and discussing simple but informative schematic cases. Applying this method in a realistic SN context will be left to future work.

Our study in Sec. II leads to the linearized equations of motion at a large distance from the neutrino source in the two-flavor case, with an azimuthally symmetric neutrino emission. In Sec. III, we present the stability analysis in the single-angle approximation, and illustrate it in Sec. IV with the examples of box spectra where the results may be understood analytically. In Sec. V we point out some special features of realistic spectra that do not vanish at low energies. Sections VI and VII demonstrate how the single-angle results are modified by the inclusion of multi-angle and matter effects. The latter one also analyzes a realistic SN spectrum using the

insights obtained from the box spectra. In Sec. VIII, we show that a multi-angle spectrum with a zero crossing is unstable in both hierarchies if the lepton asymmetry is small. In Sec. IX we conclude with a brief summary of our findings and an outlook on future directions.

II. EQUATIONS OF MOTION

A. Effective Hamiltonian

We write the EoMs in terms of $n_F \times n_F$ matrices of occupation numbers [7, 31], where n_F is the number of flavors. We denote these matrices by $\varrho_{E,\mathbf{v}}$, where the velocity vector \mathbf{v} with $|\mathbf{v}| = 1$ describes the direction of motion and the energy E is taken to be positive for neutrinos and negative for antineutrinos. Also, while the diagonal entries are equal to the occupation numbers for neutrinos, they are the negative occupation numbers for antineutrinos. In the context of a Boltzmann collision equation for mixed neutrinos, one uses positive occupation numbers in both cases and describe each mode by its momentum \mathbf{p} [7]. Our choice of signs, however, allows us to include neutrinos and antineutrinos on the same footing and we will never have to distinguish between them: The antineutrino spectrum is simply a continuation of the neutrino spectrum to negative energies. In the language of flavor polarization vectors, our convention agrees with the neutrino flavor isospin construction [14].

The EoMs for the time evolution in a homogeneous medium are

$$i\partial_t \varrho_{E,\mathbf{v}} = [\mathbf{H}_{E,\mathbf{v}}, \varrho_{E,\mathbf{v}}]. \quad (1)$$

We use sans-serif letters for matrices in flavor space. The Hamiltonian matrix is

$$\begin{aligned} \mathbf{H}_{E,\mathbf{v}} = & \frac{\mathbf{M}^2}{2E} + \sqrt{2} G_F \mathbf{N}_\ell \\ & + \sqrt{2} G_F \int_{-\infty}^{+\infty} dE' \int d\mathbf{v}' \frac{E'^2}{(2\pi)^3} \varrho_{E',\mathbf{v}'} (1 - \mathbf{v} \cdot \mathbf{v}') \end{aligned} \quad (2)$$

where \mathbf{M}^2 is the neutrino mass-squared matrix and \mathbf{N}_ℓ the matrix of net charged-lepton densities which in the flavor basis is $\mathbf{N}_\ell = \text{diag}(n_e - n_{\bar{e}}, n_\mu - n_{\bar{\mu}}, n_\tau - n_{\bar{\tau}})$. In an isotropic medium, the $\mathbf{v} \cdot \mathbf{v}'$ term drops out and the neutrino-neutrino term has the same structure as the matter term: The phase-space integral over $\varrho_{E,\mathbf{v}}$ amounts to the difference between neutrino and antineutrino densities. In the presence of macroscopic matter fluxes, there would also be current contributions in the matter term [30].

B. Azimuthal symmetry

Henceforth we assume azimuthal symmetry around some preferred direction, usually the radial direction in

the SN case. The azimuthal integration provides

$$1 - \mathbf{v} \cdot \mathbf{v}' \rightarrow 1 - v \cdot v', \quad (3)$$

where v and v' are the components of \mathbf{v} and \mathbf{v}' , respectively, along the symmetry direction. Thus $v = \cos \vartheta$ with ϑ the trajectory angle relative to the symmetry direction.

Following the Appendix of Ref. [27] we consider the EoMs expressed in terms of the radial coordinate. We introduce an arbitrary sphere with radius R that we call neutrino sphere where we specify the inner boundary condition for neutrinos that are assumed to stream only outward. Every angular mode is described by its emission angle ϑ_R relative to the radial direction at that sphere (Fig. 3 of Ref. [20]) in terms of the variable $u = \sin^2 \vartheta_R$ which lies in the range $0 \leq u \leq 1$. The u variable has the property that the modes are uniformly distributed on $0 \leq u \leq 1$ if the emission at the neutrino sphere is isotropic into space in analogy to blackbody emission.

At radius r , the radial velocity of a mode with angular label u is

$$v_{u,r} = \sqrt{1 - \frac{R^2}{r^2} u}. \quad (4)$$

In analogy to Ref. [27] we introduce the matrices

$$\Phi_{E,u,r} = \frac{r^2 E^2}{2\pi} \varrho_{E,u,r}, \quad (5)$$

where we have included a factor $4\pi r^2$, so that the integrated quantity

$$\Phi_r = \int_{-\infty}^{+\infty} dE \int_0^1 du \Phi_{E,u,r} \quad (6)$$

represents the flux through a sphere of radius r whose trace is conserved.

The EoMs for the flux matrices as a function of radial coordinate are

$$i\partial_r \Phi_{E,u,r} = [\mathbf{H}_{E,u,r}, \Phi_{E,u,r}] \quad (7)$$

with the Hamiltonian

$$\begin{aligned} \mathbf{H}_{E,u,r} &= \left(\frac{M^2}{2E} + \sqrt{2} G_F \mathbf{N}_\ell \right) \frac{1}{v_{u,r}} \\ &+ \frac{\sqrt{2} G_F}{4\pi r^2} \int_0^1 du' \left(\frac{1}{v_{u,r} v_{u',r}} - 1 \right) \Phi_{u',r}, \end{aligned} \quad (8)$$

where $\Phi_{u,r} = \int_{-\infty}^{+\infty} dE \Phi_{E,u,r}$.

C. At a large distance from source

We are interested in the evolution far away from the neutrino sphere where the flavor conversions are expected to begin. Therefore, we use the expansion

$$v_{u,r}^{-1} = 1 + \frac{u}{2} \frac{R^2}{r^2}. \quad (9)$$

Moreover, we introduce the dimensionless matrices $\mathbf{L} = \mathbf{N}_\ell / (n_e - n_{\bar{e}})$ and $\mathbf{F}_{E,u,r} = \Phi_{E,u,r} / \Phi_{\bar{\nu}_e}(R)$. Note that we normalize the charged-lepton density to the local net electron density, whereas the neutrino flux matrices are normalized to the total $\bar{\nu}_e$ flux $\Phi_{\bar{\nu}_e}(R)$ at the neutrino sphere. If we use the flavor basis, with these normalizations we have $\mathbf{L}^{ee} = 1$ and $\int_{-\infty}^0 dE \int_0^1 du \mathbf{F}_{E,u,r}^{ee} = -1$ for all r where oscillations have not yet begun.

We also introduce the coefficients with dimension of inverse energy

$$\begin{aligned} \tilde{\lambda}_r &= \sqrt{2} G_F [n_e(r) - n_{\bar{e}}(r)], \\ \mu_R &= \frac{\sqrt{2} G_F \Phi_{\bar{\nu}_e}(R)}{4\pi R^2}. \end{aligned} \quad (10)$$

In terms of these coefficients, we have

$$i\partial_r \mathbf{F}_{E,u,r} = [\mathbf{H}_{E,u,r}, \mathbf{F}_{u,r}], \quad (11)$$

with

$$\begin{aligned} \mathbf{H}_{E,u,r} &= \left(\frac{M^2}{2E} + \tilde{\lambda}_r \mathbf{L} \right) \left(1 + \frac{u}{2} \frac{R^2}{r^2} \right) \\ &+ \mu_R \frac{R^4}{r^4} \int_0^1 du' \frac{u+u'}{2} \mathbf{F}_{u',r} \end{aligned} \quad (12)$$

as the Hamiltonian at the lowest-order in (R/r) , with $\mathbf{F}_{u,r} = \int_{-\infty}^{+\infty} dE \mathbf{F}_{E,u,r}$. The first line on the right hand side of Eq. (12) is the ‘‘vacuum plus matter’’ Hamiltonian $\mathbf{H}_{E,u,r}^{\text{vac+mat}}$ while the second line is the neutrino-neutrino Hamiltonian $\mathbf{H}_{E,u,r}^{\nu\nu}$.

D. Two-flavor case

For the rest of this paper, we restrict ourselves to the two-flavor scenario, with flavors e and x , and we introduce the variable $\omega = |\Delta m^2|/2E$, the vacuum oscillation frequency, to describe the different modes. In the context of flavor oscillation physics, ω is a much more natural variable to describe the neutrino spectrum than the energy E . Note that since E is taken to be negative for antineutrinos, they are represented by negative ω values. Since the trace of the Hamiltonian does not contribute to the time evolution, we write

$$\begin{aligned} \frac{M^2}{2E} &= \pm \frac{\omega}{2} \begin{pmatrix} \cos 2\theta & \sin 2\theta \\ -\sin 2\theta & -\cos 2\theta \end{pmatrix}, \\ \tilde{\lambda}_r \mathbf{L} &= \frac{\tilde{\lambda}_r}{2} \begin{pmatrix} 1 & 0 \\ 0 & -1 \end{pmatrix}, \end{aligned} \quad (13)$$

in the flavor basis, after removing a term proportional to the unit matrix. We take the mixing angle θ to lie in the first octant $0 < \theta < \pi/4$. In this case the $+(-)$ sign stands for inverted (normal) mass hierarchy. In the following discussion, we shall consider inverted hierarchy. For obtaining results with normal hierarchy, we will have to multiply the ω term by a factor of -1 .

The flux matrices at the neutrino sphere are

$$\mathbf{F}_{\omega,u,R} = \begin{pmatrix} \phi_{\omega,u}^e & 0 \\ 0 & \phi_{\omega,u}^x \end{pmatrix}, \quad (14)$$

where the $\phi_{\omega,u}$ are differential fluxes in the variables ω and u . The normalization of \mathbf{F} used here implies that $\int_{-\infty}^0 d\omega \int_0^1 du \phi_{\omega,u}^e = -1$. Note that $\phi_{\omega,u}$ for antineutrinos ($\omega < 0$) corresponds to the negative of their occupation numbers. Finally, in the flavor basis we write

$$\mathbf{F}_{\omega,u,r} = \frac{\text{Tr} \mathbf{F}_{\omega,u,r}}{2} + \frac{g_{\omega,u}}{2} S_{\omega,u,r}, \quad (15)$$

where $g_{\omega,u} = \phi_{\omega,u}^e - \phi_{\omega,u}^x$ is the usual difference spectrum, except that it is now also differential with regard to the direction variable u . The initial conditions at the neutrinosphere for the Hermitian matrix $S_{\omega,u,r}$ are

$$S_{\omega,u,R} = \begin{pmatrix} 1 & 0 \\ 0 & -1 \end{pmatrix}. \quad (16)$$

It satisfies the EoMs

$$i\partial_r S_{\omega,u,r} = [H_{E,u,r}, S_{\omega,u,r}] \quad (17)$$

with the neutrino-neutrino part of the Hamiltonian

$$H_{\omega,u,r}^{\nu\nu} = \mu_r \int_0^1 du' (u+u') \int_{-\infty}^{+\infty} d\omega' \frac{g_{\omega'u'}}{2} S_{\omega',u',r} \quad (18)$$

and

$$\mu_r = \mu_R \frac{R^4}{2r^4}. \quad (19)$$

The effective neutrino-neutrino interaction energy declines with r^{-4} .

E. In a co-rotating frame

We go to a rotating frame where the common matter term drops out and where the vacuum term oscillates quickly, averaging the off-diagonal term to zero [30]. Moreover, in the large- r limit we ignore a small radius-dependent shift of ω . Then we find

$$H_{\omega,u,r}^{\text{vac+mat}} = \frac{\omega + u\lambda_r}{2} \begin{pmatrix} 1 & 0 \\ 0 & -1 \end{pmatrix}, \quad (20)$$

where

$$\lambda_r = \tilde{\lambda}_r \frac{R^2}{2r^2} = \sqrt{2} G_F [n_e(r) - n_{\bar{e}}(r)] \frac{R^2}{2r^2} \quad (21)$$

encodes the net matter effect. Note that the $1/r^2$ variation here has nothing to do with the matter density profile, the effect of the latter appears through the $n_e(r)$ term.

Next we write the S matrices in components in the flavor basis

$$S_{\omega,u,r} = \begin{pmatrix} s_{\omega,u,r} & S_{\omega,u,r} \\ S_{\omega,u,r}^* & -s_{\omega,u,r} \end{pmatrix}, \quad (22)$$

where $s_{\omega,u,r}$ is the r -dependent swap factor. It specifies how much the flavor content of the given mode has been swapped relative to the initial condition. We have the normalization $s_{\omega,u,r}^2 + |S_{\omega,u,r}|^2 = 1$. Likewise,

$$H_{\omega,u,r} = \begin{pmatrix} h_{\omega,u,r} & H_{\omega,u,r} \\ H_{\omega,u,r}^* & -h_{\omega,u,r} \end{pmatrix}. \quad (23)$$

Then the EoM for the off-diagonal component is

$$i\partial_r S_{\omega,u,r} = 2(h_{\omega,u,r} S_{\omega,u,r} - s_{\omega,u,r} H_{\omega,u,r}). \quad (24)$$

The components of the Hamiltonian matrix are explicitly

$$\begin{aligned} h_{\omega,u,r} &= \frac{\omega + u\lambda_r}{2} \\ &+ \frac{\mu_r}{2} \int_0^1 du' (u+u') \int_{-\infty}^{+\infty} d\omega' g_{\omega'u'} s_{\omega',u',r}, \\ H_{\omega,u,r} &= \frac{\mu_r}{2} \int_0^1 du' (u+u') \int_{-\infty}^{+\infty} d\omega' g_{\omega'u'} S_{\omega',u',r}. \end{aligned} \quad (25)$$

In the absence of all interactions, the rotation-averaged EoM is

$$i\partial_r S_{\omega,u,r} = \omega S_{\omega,u,r}, \quad (26)$$

implying the free precession solution

$$S_{\omega,u,r} = e^{-i\omega(r-R)} S_{\omega,u,R}. \quad (27)$$

F. Small-amplitude expansion

Henceforth we drop the explicit subscript r to denote the r -dependence of all quantities. Moreover, we drop the limits of integration which are always as above. In the small-amplitude case we have $s_{\omega,u} = 1$. This simplifies in particular the diagonal Hamiltonian term which is

$$h_{\omega,u} = \frac{\omega + u\lambda}{2} + \frac{\mu}{2} \int du' (u+u') \int d\omega' g_{\omega'u'}. \quad (28)$$

In the neutrino-neutrino term, the integral which involves $\int du'u' \dots$ is a constant that does not depend on ω or u and therefore amounts to a shift of all frequencies, i.e. yet another rotating frame. Once more we can drop this term and are left with

$$h_{\omega,u} = \frac{\omega + u(\lambda + \epsilon\mu)}{2}. \quad (29)$$

Here,

$$\epsilon = \int du d\omega g_{\omega,u} \quad (30)$$

quantifies the ‘‘asymmetry’’ or ‘‘total lepton number’’ of the neutrino spectrum, normalized to the total $\bar{\nu}_e$ flux. The EoMs are then explicitly

$$i\partial_r S_{\omega,u} = [\omega + u(\lambda + \epsilon\mu)] S_{\omega,u} - \mu \int du' d\omega' (u + u') g_{\omega'u'} S_{\omega',u'}. \quad (31)$$

This is the linearized form of the EoMs and provides the starting point for the stability analysis.

At this point it may be useful to recapitulate the elements that have gone into this analysis. Besides the small-amplitude approximation $|S_{\omega,u}| \ll 1$, we have taken the neutrinos to be far away from the neutrino sphere, $R/r \ll 1$. At the same time, they have not yet reached the MSW resonance region, so that the ordinary matter effect is large and the effective mixing angle in matter is small. We have also assumed that the vacuum mixing angle is so small that we may approximate $\cos\theta = 1$, but it is trivial to accommodate another choice. We have assumed that the fast-rotating off-diagonal component of the Hamiltonian matrix caused by the mismatch between the mass and flavor directions averages to zero, so the only off-diagonal contribution of the Hamiltonian is provided by the neutrinos themselves. In numerical simulations, this fast-rotating component provides the initial disturbance to kick-start exponentially growing modes. Here, however, we do not ask how the instability gets started, we only ask for the existence of exponentially growing modes.

G. Eigenvalue equation

The stability analysis determines if the small quantities $S_{\omega,u}$ grow exponentially with r . This is achieved by writing $S_{\omega,u}$ as

$$S_{\omega,u} = Q_{\omega,u} e^{-i\Omega r}, \quad (32)$$

where both $Q_{\omega,u}$ and Ω are in general complex numbers. A purely real solution for Ω would imply that all modes precess with a common frequency. A complex solution $\Omega \equiv \gamma + i\kappa$, with $\kappa > 0$, would indicate an exponentially increasing $S_{\omega,u}$, i.e., an instability. On the other hand, $\kappa < 0$ would indicate that the solution decreases exponentially toward the asymptotic solution $S_{\omega,u} = 0$.

In terms of $Q_{\omega,u}$, the EoM becomes

$$(\omega + u\bar{\lambda} - \Omega)Q_{\omega,u} = \mu \int du' d\omega' (u + u') g_{\omega'u'} Q_{\omega',u'}, \quad (33)$$

where $\bar{\lambda} \equiv \lambda + \epsilon\mu$. This may be looked upon as an eigenvalue equation for $Q_{\omega,u}$, which is a vector in the function space on the ω - u plane, with the eigenvalue Ω . The eigenfunction $Q_{\omega,u}$ implicitly carries a label Ω because usually for every Ω there exists a different $Q_{\omega,u}$. Note that if $Q_{\omega,u}$ and its corresponding Ω satisfies Eq. (33), so

does $Q_{\omega,u}^*$ with the eigenvalue Ω^* . This implies that for each complex solution for $\Omega = \gamma + i\kappa$, there exists another solution $\Omega = \gamma - i\kappa$. Thus, the exponentially increasing and decreasing solutions always appear in pairs.

III. SINGLE-ANGLE STABILITY ANALYSIS

A. The consistency conditions

Many important features of collective neutrino oscillation phenomena can be understood in a simplified model where only a single angular mode $u = u_0$ is occupied, i.e., all neutrinos are assumed to be emitted from the neutrino sphere at a fixed angle relative to the radial direction. We therefore first perform the stability analysis with this assumption and later extend it to the multi-angle case. In the simplest schematic SN model, the neutrino sphere at radius R is pictured as a blackbody source without limb darkening, in which case the angular distribution is such that u is uniformly distributed on the interval $0 \leq u \leq 1$. It is natural to represent this case in the single-angle approximation by $u_0 = 1/2$. For the time being, however, we keep u_0 as a free parameter.

Since $u = u_0$, the term $u\bar{\lambda}$ in the EoM corresponds to a common precession for all modes. We therefore can go to a basis rotating with frequency $u_0\bar{\lambda}$, in which Eq. (31) becomes

$$i\partial_r S_\omega = \omega S_\omega - 2u_0\mu \int d\omega' g_{\omega'} S_{\omega'}. \quad (34)$$

The single-angle approximation is then equivalent to saying that all the neutrinos feel the same refractive effect due to the other neutrinos. Requiring the solution to be of the form $S_\omega = Q_\omega e^{-i\Omega r}$ gives

$$(\omega - \Omega) Q_\omega = 2u_0\mu \int d\omega' g_{\omega'} Q_{\omega'}. \quad (35)$$

This is the single-angle form of the eigenvalue equation in Eq. (33).

For the l.h.s. of the eigenvalue equation to be independent of ω like the r.h.s., we must have

$$Q_\omega \propto \frac{1}{\omega - \Omega} \quad (36)$$

and therefore

$$\mu^{-1} = 2u_0 \int d\omega \frac{g_\omega}{\omega - \Omega}. \quad (37)$$

For an instability, this equation should have a complex root $\Omega = \gamma + i\kappa$. Then, splitting the equation into real and imaginary part, one obtains the two equations

$$(2u_0\mu)^{-1} = \int d\omega g_\omega \frac{\omega - \gamma}{(\omega - \gamma)^2 + \kappa^2}, \quad (38)$$

$$0 = \int d\omega g_\omega \frac{\kappa}{(\omega - \gamma)^2 + \kappa^2}. \quad (39)$$

Eqs. (38) and (39) are the conditions that must be simultaneously satisfied by γ and the positive quantity κ^2 . If a solution exists, we automatically have a pair of solutions $\Omega = \gamma \pm \pm i|\kappa|$, of which one corresponds to an instability that will grow at the rate $e^{|\kappa|t}$.

When an instability occurs, $|Q_\omega|^2$ takes the form of a Lorentzian centered at $\omega = \gamma$ and half-width characterized by κ . Thus, the solutions for γ and κ tell us the range of ω -modes which are significantly affected. We therefore present our results in the form of the parameters γ and κ . Note that significant flavor transformations take place only if g_ω is significant in this range.

In the form of Eqs. (38) and (39), these results were previously derived in Ref. [19] where the full solution was provided, not only the small-amplitude expansion. The exponentially growing and shrinking solutions correspond to the “flavor pendulum” near its inverted position close to the beginning or end of a full swing. A purely real Ω (no exponential growth) corresponds to the pure precession mode [15, 16, 23]. While Eqs. (38) and (39) are not new, the linearized analysis illustrates the origin of the Lorentz denominator in the eigenfunction Q_ω .

A pure precession mode is described by a real eigenvalue $\Omega = \gamma$. In this case Q_ω becomes singular for $\omega = \gamma$ and the small-amplitude expansion is not self-consistent if $g(\gamma) \neq 0$. The full non-singular self-consistency relation for the pure precession mode, without the small-amplitude approximation, was provided in Ref. [15] and of course agrees in the appropriate limit. The linearized equations are useful to study the presence of instabilities, but not necessarily to study the pure precession solutions.

B. A single spectral zero crossing

The conditions in Eqs. (38) and (39) allow us to understand some of the stability features analytically. For example, for the integral in Eq. (39) to vanish, the integrand has to be positive in some parts and negative in the other. Thus, an instability requires the spectrum g_ω to have a zero-crossing. The existence of such an instability also requires the spectrum to cross from negative to positive values [19].

During the accretion phase of SN evolution, powerful ν_e and $\bar{\nu}_e$ fluxes are emitted, with a much weaker flux of other flavors. If we model this situation by a pure Fermi-Dirac spectrum of e -flavored neutrinos in the inverted hierarchy, the spectrum is positive for ν_e and negative for $\bar{\nu}_e$, providing for a single-crossed spectrum (Fig. 1). Therefore, instabilities are a generic feature of the neutrino flux streaming from a SN core.

Note that in the limit $\kappa \rightarrow 0$, the integrand in Eq. (39) becomes $g_\omega \pi \delta(\omega - \gamma)$. Therefore, the consistency condition implies $g(\gamma) = 0$. Thus in this limit, the instability starts near the zero crossing. Also, the r.h.s. of Eq. (38) gets a large contribution from the modes $\omega \approx \gamma$, implying a small μ . Therefore in the single-angle approximation, at small neutrino density one generically gets a narrow

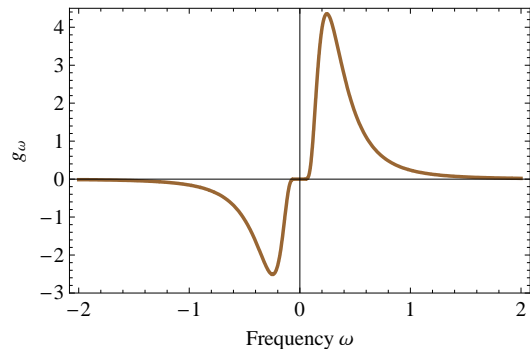


FIG. 1: Fermi-Dirac spectrum for ν_e and $\bar{\nu}_e$, with $\Delta m^2 = 1$, and $T = 1$ for both species. A small degeneracy parameter $\eta = 0.28$ provides an excess flux of ν_e over $\bar{\nu}_e$, which corresponds to $\epsilon = 0.666$.

instability centered at a positive crossing.

C. Normal vs. inverted hierarchy

Recall that all our results have been obtained using inverted hierarchy. Going to normal hierarchy corresponds to changing Eq. (34) to

$$i\partial_r \tilde{S}_\omega = -\omega \tilde{S}_\omega - 2u_0 \mu \int d\omega' g_{\omega'} \tilde{S}_{\omega'}. \quad (40)$$

In terms of the solution S_ω of Eq. (34), the solution of this equation is given by

$$\tilde{S}_\omega(\mu, g_\omega) = S_\omega^*(\mu, -g_\omega) = S_\omega^*(-\mu, g_\omega). \quad (41)$$

Since S and S^* should have the same stability behavior, this implies that the stability conditions for normal hierarchy are the same as those for the inverted hierarchy with a change in the sign of g_ω .

Formally we may implement this change of sign by keeping the same g_ω and $\mu \rightarrow -\mu$. In this sense one can show the solutions $\kappa(\mu)$ and $\gamma(\mu)$ on the same plot for both hierarchies by extending it to negative values of μ .

D. Multiple spectral crossings

A supernova emits neutrinos of all flavors, although with different fluxes and spectra. As g_ω is the difference spectrum between ν_e and ν_x , usually there will be additional spectral crossings other than the one at $\omega = 0$. In the limit $\mu \rightarrow 0$ and concomitant $\kappa \rightarrow 0$, there will be a solution Q_ω centered on every positive crossing as already stressed in Ref. [19]. For larger μ there can be fewer solutions, but if there are several, they can coexist even when the different eigenfunctions are not well separated.

In the single-angle case, our problem is equivalent to the reduced pairing Hamiltonian which is at the core of

the BCS theory of superconductivity [32]. In this context, the same stability problem was recently investigated and it was shown how general analytic solutions can be constructed [33]. In other words, explicit large-amplitude solutions were constructed that correspond to several co-existing solutions with different Ω -values. The single- Ω large-amplitude solution of Ref. [19] is the simplest case of the class of multiple “normal soliton solutions.”

IV. BOX-SPECTRA EXAMPLES

In order to understand the behavior of the stability criteria it is useful to study explicit examples of single and multi-crossed spectra that can be solved analytically. The simplest approach is to represent a spectrum such as Fig. 1 in the single-energy approximation by one δ function for one average ω (neutrinos) and one for negative ω (antineutrinos), or more such spikes to represent a multi-crossed spectrum. One then finds simple polynomial equations for Ω with coefficients that depend on the frequencies and heights of the spikes.

We here go one step further and represent the spectra by “boxes” of unit height, i.e. g_ω only takes the values $0, \pm 1$. This makes the integral in Eq. (35) once more analytically calculable and Ω becomes the root of a polynomial whose degree depends on the number of boxes. As will be seen, the simplified box spectra already bring out some important features of the stability of the realistic SN spectra.

Scaling the height of all the boxes by a factor α corresponds to scaling the spectrum as $g_\omega \rightarrow \alpha g_\omega$. The results for this may be obtained by simply scaling $\mu \rightarrow \alpha\mu$. For the sake of simplicity, in the analytic single-angle arguments we use $u_0 = 1/2$. The results for any u_0 may be obtained by the scaling $\mu \rightarrow 2u_0\mu$. The numerical results are given for various sample u_0 values.

A. Two boxes

Our first example is a schematic representation of the Fermi-Dirac spectrum of Fig. 1. We define our two-box spectrum as

$$g_\omega = \begin{cases} -1 & -a < \omega < 0 \\ +1 & 0 < \omega < b \end{cases} \quad (42)$$

as shown in Fig. 2. We assume that all frequencies are normalized to some common frequency scale. The consistency condition in Eq. (35) yields

$$\frac{\Omega^2}{(\Omega + a)(\Omega - b)} = \eta, \quad (43)$$

where $\eta \equiv e^{-1/\mu}$. This corresponds to the quadratic equation

$$(1 - \eta)\Omega^2 + (b\eta - a\eta)\Omega + ab\eta = 0, \quad (44)$$

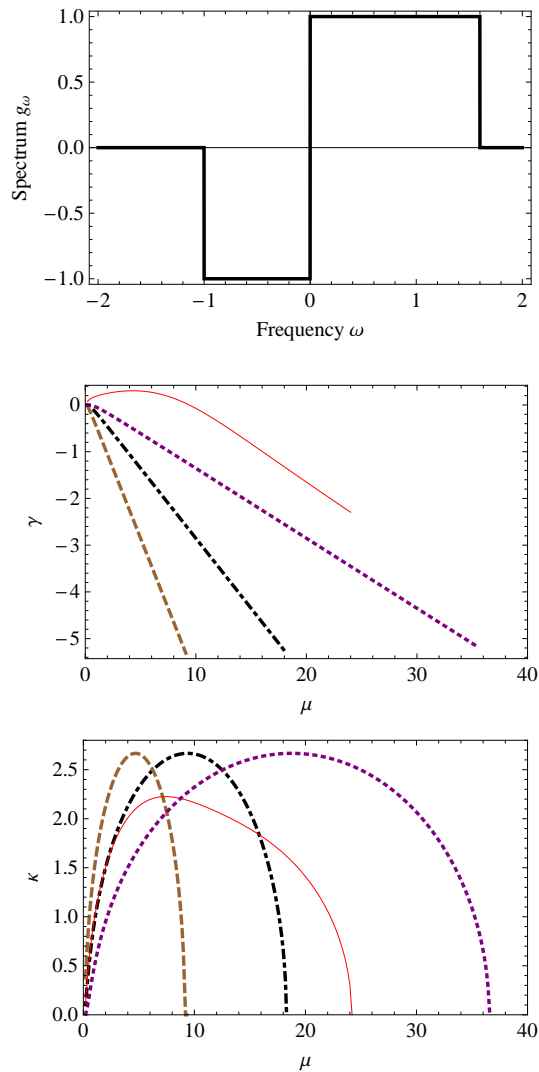


FIG. 2: Two-box spectrum with $a = 1$ and $b = 1.6$. Lower panels: $\gamma(\mu)$ and $\kappa(\mu)$, where broken curves are single angle with $u_0 = 1, 1/2$ and $1/4$ (left to right). Thin solid (red) line: Multi-angle with uniform distribution $0 \leq u \leq 1$. Solutions for $\gamma(\mu)$ are only shown where $\kappa(\mu) \neq 0$.

from which the stability can be analyzed analytically. Note that $0 < \eta < 1$, while the limits $\mu \rightarrow \infty$ and $\mu \rightarrow 0$ correspond to $\eta = 1$ and $\eta = 0$, respectively.

The roots of Eq. (44) are

$$\Omega = \frac{-(b - a)\eta \pm \sqrt{(b - a)^2\eta^2 - 4ab\eta(1 - \eta)}}{2(1 - \eta)}. \quad (45)$$

We have two complex conjugate solutions when the argument of the square-root is negative, i.e. for

$$0 < \eta < \eta_{\text{sync}} \equiv \frac{4ab}{(b + a)^2}. \quad (46)$$

Here η_{sync} is the “synchronization strength,” i.e. for a larger interaction strength the system is stuck in a stable

position. If $0 < \eta < \eta_{\text{sync}}$, we find

$$\begin{aligned}\gamma &= -\frac{(b-a)\eta}{2(1-\eta)}, \\ \kappa &= \pm \frac{\sqrt{4ab\eta(1-\eta) - (b-a)^2\eta^2}}{2(1-\eta)}.\end{aligned}\quad (47)$$

These solutions are shown in Fig. 2 for a spectrum with $a = 1$, $b = 1.6$, and different values of the single emission angle u_0 .

For $\eta > \eta_{\text{sync}}$ the solutions for Ω are two different real roots so that $\kappa = 0$. At the synchronization strength η_{sync} , we find

$$\gamma_{\text{sync}} = -\frac{2ab}{(b-a)}.\quad (48)$$

In our figures we only show the solutions with nonvanishing κ , since when $\kappa = 0$, the complex solutions $\gamma \pm i\kappa$ do not exist and there are no instabilities. Therefore, the $\gamma(\mu)$ curves are only shown where $\kappa(\mu) \neq 0$.

At the vanishing interaction strength $\mu = 0$, we have $\gamma = \kappa = 0$. Had we put a spectral gap between the two boxes, the lower- μ cutoff point would be at a nonzero interaction strength $\mu > 0$.

For the completely antisymmetric two-box spectrum ($a = b$), Eq. (44) reduces to

$$\Omega^2 = -\frac{ab\eta}{1-\eta},\quad (49)$$

which always has purely imaginary solutions. Thus, there is no synchronized behavior for such a spectrum, the flavor conversions take place at arbitrarily high values of μ . We will not further consider this special case that requires a fine-tuned spectrum. Moreover, a SN core always produces an excess flux of ν_e over $\bar{\nu}_e$ due to deleptonization.

The spectrum shown in Fig. 2 has a positive zero-crossing. The case of a negative zero-crossing may be studied by multiplying the spectrum g_ω by a factor of -1 , i.e. $g_\omega \rightarrow -g_\omega$. The consistency conditions then stay the same, with the change $\mu \rightarrow -\mu$, or $\eta \rightarrow 1/\eta$. Equation (44) then becomes

$$(1-\eta)\Omega^2 - (b-a)\Omega - ab = 0,\quad (50)$$

which always has real roots. Thus, the spectrum is stable as anticipated from our earlier arguments.

To summarize, for the two-box spectrum in the single-angle approximation, the spectrum with a positive zero-crossing is always stable in the normal hierarchy. In the inverted hierarchy (i) the spectrum with a negative zero-crossing is always stable, (ii) a completely antisymmetric spectrum with a positive zero-crossing is unstable at any value of μ , (iii) an asymmetric spectrum with a positive zero-crossing is stable above a threshold value of the interaction strength and unstable if the interaction strength is smaller.

B. Three boxes

The natural next case is a spectrum with two crossings, of which only one can be positive, and so we expect at most one unstable solution for the eigenvalue equation. However, it was recognized earlier that such a spectrum shows additional features in that $\kappa(\mu)$ need not cut off at large μ [28].

We represent this case by three adjacent equal-height boxes of the form (Fig. 3)

$$g_\omega = \begin{cases} -1 & -a < \omega < 0 \\ +1 & 0 < \omega < b \\ -1 & b < \omega < c \end{cases}.\quad (51)$$

The consistency condition in Eq. (35) leads to the cubic equation

$$\begin{aligned}(1-\eta)\Omega^3 - (c-2b\eta+a\eta)\Omega^2 \\ -(b^2-2ab)\eta\Omega - ab^2\eta = 0.\end{aligned}\quad (52)$$

It can have three real roots, or a single real root and a pair of complex conjugate roots. The latter case corresponds to instability.

In order to study the stability at large μ , we look at the limit $\eta = 1$. The cubic term in Eq. (52) drops out, leaving us with the quadratic equation

$$(a-2b+c)\Omega^2 + (b^2-2ab)\Omega + ab^2 = 0.\quad (53)$$

When the total lepton number is not zero ($2b-a-c \neq 0$) the solutions are

$$\Omega = \frac{2ab-b^2 \pm \sqrt{b(4ab+b^2-4ac)}}{2(a-2b+c)}.\quad (54)$$

If $4ab+b^2-4ac > 0$ then both roots are real, implying that the system is stable. We then get the same cutoff behavior as in the two-box case, similar to the one shown in Fig. 2.

On the other hand, if $4ab+b^2-4ac < 0$, and writing $\Omega = \gamma \pm i\kappa$, we find

$$\gamma = \frac{2ab-b^2}{2(a-2b+c)}, \quad \kappa = \frac{\sqrt{b(4ac-b^2-4ab)}}{2(a-2b+c)}.\quad (55)$$

Thus κ reaches a non-zero asymptotic saturation value that is independent of μ . Likewise, γ approaches a μ -independent asymptotic value, implying that the eigenfunction Q_ω remains roughly centered on the nonvanishing spectral range. The system is thus unstable even at large μ values. This saturation behavior, shown in Fig. 3, was absent in the two-box scenario. This would allow flavor conversions to start deep inside the SN core.

The spectrum in Fig. 3 has its central box positive. The corresponding spectrum with the central box negative can be treated in the same manner, with the replacement $g_\omega \rightarrow -g_\omega$, which corresponds to $\mu \rightarrow -\mu$ or $\eta \rightarrow 1/\eta$. In the $\eta = 1$ limit (large neutrino density) the behavior is then identical with the one described above.

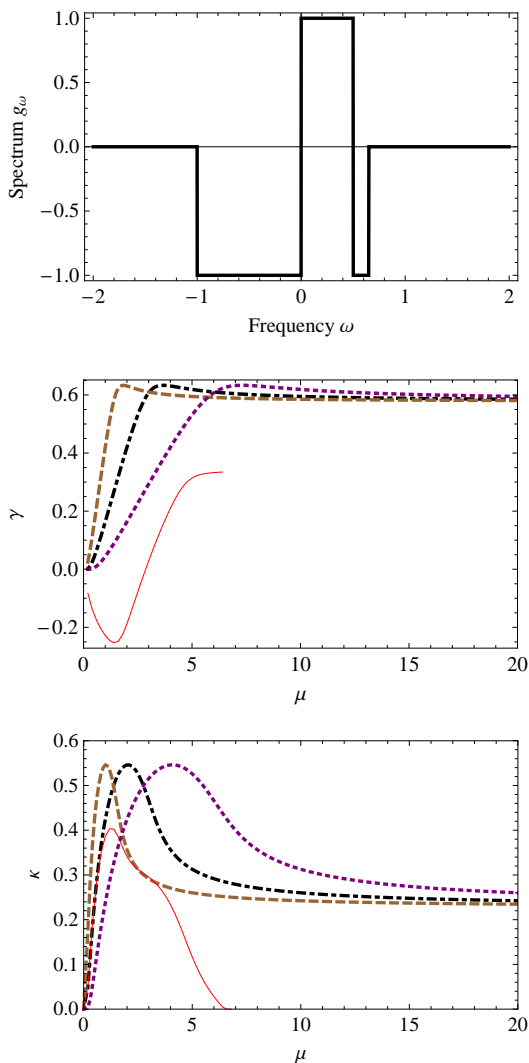


FIG. 3: Three-box spectrum with $a = 1, b = 0.5, c = 0.6$. Lower panels: $\gamma(\mu)$ and $\kappa(\mu)$, where broken curves are single angle with $u_0 = 1, 1/2$ and $1/4$ (left to right). Thin solid (red) line: Multi-angle with uniform distribution $0 \leq u \leq 1$. Solutions for $\gamma(\mu)$ are only shown where $\kappa(\mu) \neq 0$.

When the total lepton number vanishes, Eq. (52) reduces to

$$(1 - \eta)\Omega^3 - (2b - a)(1 - \eta)\Omega^2 - (b^2 - 2ab)\eta\Omega - ab^2\eta = 0. \quad (56)$$

One can examine if it has three roots of the form $\Omega_1, \Omega_2 = \gamma + i\kappa, \Omega_3 = \gamma - i\kappa$ in the limit $\eta = 1$. Clearly in this limit, $\Omega_1 = ab/(2a - b)$ is a real finite root. Then the sum of the roots is $\Omega_1 + 2\gamma = 2b - a$, a finite number, implying that γ is finite. On the other hand, the product of the roots, $\Omega_1(\gamma^2 - \kappa^2) = -ab^2\eta/(1 - \eta)$ is a large negative number. This is possible only if κ is a large number, and $\Omega_1 > 0$, i.e. $2a - b > 0$. Thus, the stability in this case is determined by the sign of $(2a - b)$. If this is negative, then there is a cutoff behavior, i.e. the system is stable in the $\eta = 1$ limit. If this is positive, then the system is

unstable at arbitrarily large μ . For the inverted spectrum $g_\omega \rightarrow -g_\omega$, the condition for stability is reversed.

The three-box spectra thus show a cutoff or saturation behavior, depending on the details of the spectrum. The saturation behavior cannot occur for two boxes and is a new feature. The three-box spectra thus open up the possibility that for certain combinations of spectra and hierarchy, the neutrino ensemble is never stable. We will see, however, that this behavior is qualitatively modified by multi-angle effects.

C. Four boxes

A four-box spectrum comes closest to representing a realistic SN spectrum which typically has three zero crossings as explained earlier. Representing it by four adjacent boxes, we define the spectrum as

$$g_\omega = \begin{cases} -1 & -a < \omega < -b \\ +1 & -b < \omega < 0 \\ -1 & 0 < \omega < c \\ +1 & c < \omega < d \end{cases}. \quad (57)$$

The self consistency condition is

$$\frac{(\Omega + b)^2(\Omega - c)^2}{(\Omega + a)\Omega^2(\Omega - d)} = \eta \quad (58)$$

and can be written as

$$(1 - \eta)\Omega^4 + (2b - 2c - a\eta + d\eta)\Omega^3 + (b^2 - 4bc + c^2 + ad\eta)\Omega^2 + (2bc^2 - 2b^2c)\Omega + b^2c^2 = 0. \quad (59)$$

This quartic equation can have zero, one or two pairs of complex solutions, so this is the first explicit case with the possibility of two simultaneous unstable solutions.

We are interested in the high-density behavior where $\eta = 1$. In this limit, the quartic equation reduces to a cubic equation with real coefficients. Hence we are guaranteed at least one real root and we can have at most one pair of complex conjugate solutions, i.e. at most one solution for κ^2 . Its existence is determined by the value of the discriminant

$$\begin{aligned} \Delta = & b^2c^2[-27b^2c^2(a - 2b + 2c - d)^2 \\ & + 32b(b - c)^3c(-a + 2b - 2c + d) \\ & - 36b(b - c)c(-a + 2b - 2c + d)(b^2 - 4bc + c^2 + ad) \\ & + 4(b - c)^2(b^2 - 4bc + c^2 + ad)^2 \\ & - 4(b^2 - 4bc + c^2 + ad)^3]. \end{aligned} \quad (60)$$

If $\Delta > 0$, all the roots are real and the system is stable.

A typical scenario is shown in Fig. 4. At low μ values, there are two instabilities, one of which shows a cutoff behavior, i.e. it vanishes for μ greater than a certain value. The other instability, with $\gamma \approx 0$, survives for arbitrarily large values of μ , with κ showing a saturation behavior as

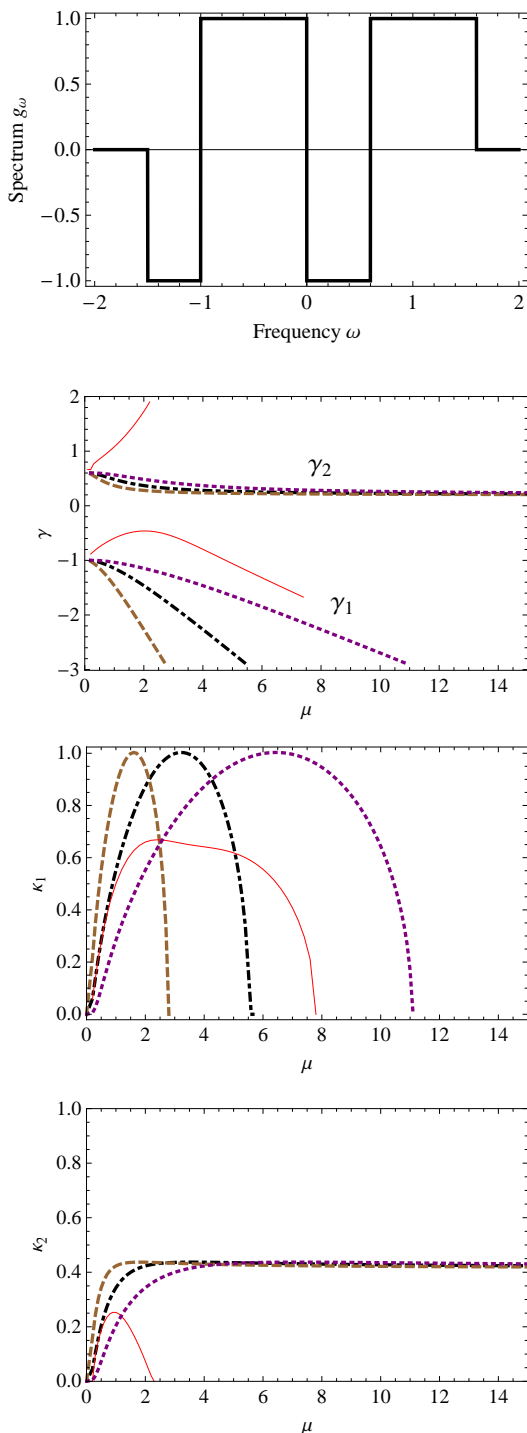


FIG. 4: Four-box spectrum with $a = 1.5$, $b = 1.0$, $c = 0.6$ and $d = 1.6$. *Lower panels:* $\gamma(\mu)$ and $\kappa(\mu)$, where the solution with larger γ is termed number 1. Broken curves are single angle with $u_0 = 1$, $1/2$ and $1/4$ (left to right). Thin solid (red) line: Multi-angle with uniform distribution $0 \leq u \leq 1$. Solutions for $\gamma(\mu)$ are only shown where $\kappa(\mu) \neq 0$.

in the 3-box case. Under the transformation $g_\omega \rightarrow -g_\omega$, $\mu \rightarrow -\mu$, $\eta \rightarrow 1/\eta$, the instability condition at $\eta = 1$ does not change, so that at large neutrino densities the saturation solution exists in either hierarchy.

The four-box spectra can give rise to two instabilities at the same time, or only one, or none at all, depending on the spectral details and strength of μ . At most one of them can show saturation behavior at large density, which then exists for both hierarchies.

V. SPECTRA WITH TAILS

The ultimate goal of our investigation in the context of SN physics is to understand in which regions of the star the neutrino stream may show self-induced instabilities. In agreement with the previous literature we have found that in some cases, and notably in the generic two-box example, there is a value μ_{sync} such that for $\mu > \mu_{\text{sync}}$ the system is stable. Upon closer scrutiny, however, one finds that the stable regime does not exist for a realistic spectrum. The main difference between the Fermi-Dirac spectrum of Fig. 1 and the two-box spectrum of Fig. 2 is that the former has nonvanishing tails for large $|\omega|$, corresponding to the infrared part of the spectrum. In other words, $g_\omega \neq 0$ everywhere except at the spectral crossing point. Given a positive spectral crossing, the only solutions with $\kappa \rightarrow 0$ can be those centered on the spectral crossing and corresponding to $\mu \rightarrow 0$. Purely real solutions for Ω then do not exist for large μ and the system is always unstable.

One can easily illustrate this point by a numerical solution of the eigenvalue equation for the Fermi-Dirac spectrum of Fig. 1. We show $\gamma(\mu)$ and $\kappa(\mu)$ in Fig. 5, assuming single angle with $u_0 = 1/2$. The result is qualitatively similar to the two-box example, except that at large μ the curve $\kappa(\mu)$ has a tail.

In a SN core, the system as a function of radius sweeps from very large μ -values (of order 10^6 in our normalization) to zero, but the system is nowhere stable. Still, the usual onset of bipolar oscillations happens approximately at the μ -value around the would-be synchronization value where the “hump” and the “tail” of the $\kappa(\mu)$ curve join, in Fig. 5 around $\mu \sim 10$ – 11 , as confirmed in numerous numerical SN examples.

The explanation is two-fold. At large μ the system is always unstable, but $\kappa(\mu)$ is very small and the exponential growth will not get anywhere on the available time scale (or rather, radial distance scale), in particular as the center of the resonance, $\gamma(\mu)$, is constantly shifting as a function of the decreasing μ . Second, the center of the resonance is far away in the spectral tail (the infrared energy modes), so only a narrow range of infrared modes is affected. It deserves mention that “small κ ” simultaneously means two things: The exponential growth is slow and the resonance width is narrow.

Evidently, then, a stability analysis alone is not enough to understand the consequences in a realistic SN. One

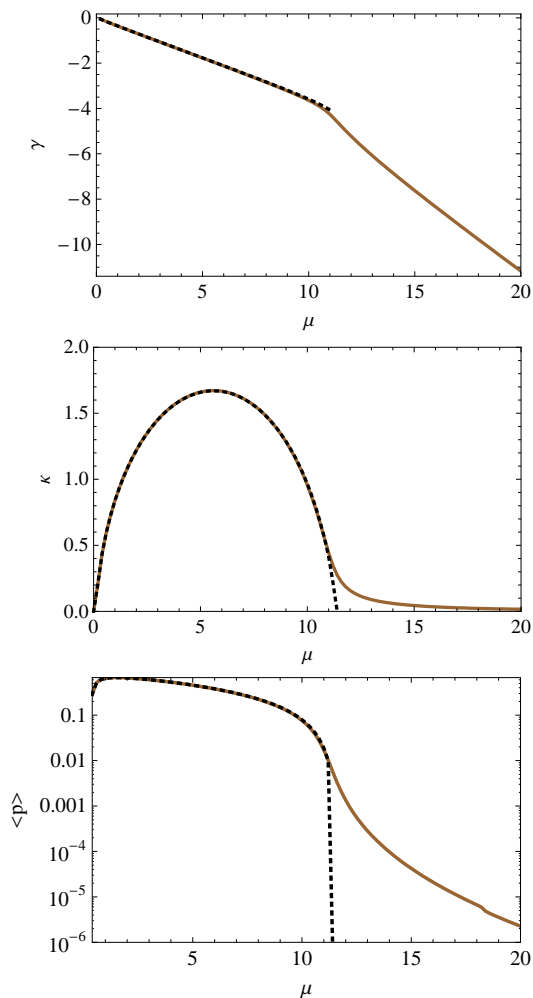


FIG. 5: Eigenvalue solution for the Fermi-Dirac spectrum of Fig. 1, shown by the brown (solid) line. As a dotted (black) line we show the same result if the Fermi-Dirac spectrum is cut off for $|\omega| > 4$. Bottom panel: $\langle p \rangle$.

needs a more dynamical approach that takes account of the available time scale as μ sweeps from large to small values, and one needs to consider the range of modes that are actually affected by the resonance.

One rough way to approach the latter point is to consider the maximum total flavor conversion that can be achieved by a solution Ω on a given spectrum, or equivalently, the average conversion probability over the entire spectrum when the flavor pendulum has moved from the inverted to the normal position. From the exact large-amplitude instantaneous solution [19] one finds that the maximum conversion probability of a mode of frequency ω is

$$p_\omega = \frac{\kappa^2}{(\omega - \gamma)^2 + \kappa^2}. \quad (61)$$

Averaged over all modes this is

$$\langle p \rangle = \frac{\int_{-\infty}^{+\infty} d\omega p_\omega |g_\omega|}{\int_{-\infty}^{+\infty} d\omega |g_\omega|}. \quad (62)$$

We can speak of an effective cutoff behavior if $\langle p \rangle$ as a function of μ quickly drops to very small values in a narrow range of μ , while being appreciably large at smaller μ . In the bottom panel of Fig. 5 we show $\langle p \rangle$ for the Fermi-Dirac example. Indeed, for $\mu \sim 11$, this measure drops by orders of magnitude and we would have an effective cutoff—above this transition range, only a minimal range of infrared modes experiences self-induced conversion.

Another approach is to artificially cut off the infrared part of the spectrum. The curve $\gamma(\mu)$ in Fig. 5 has a distinct kink exactly in the region where the the hump and tail of the $\kappa(\mu)$ curve join. If we cut off the Fermi-Dirac spectrum and set it to 0 for $|\omega| > 4$, the $\kappa(\mu)$ curve follows the original one almost exactly, except that the tail is cut off at $\mu_{\text{sync}} \sim 11$ and the system becomes perfectly stable for larger μ values (Fig. 5). Therefore, the simple picture of a cutoff behavior is actually very good except for a minor infrared correction and our study of box spectra indeed provides a useful picture of the instability behavior.

The saturation solutions that can arise for spectra with two or more crossings (three or more boxes) are very different. The saturation solutions have a κ that is comparable to the width of the spectrum and remain centered on the main part of the spectrum. Therefore, such an instability cannot be removed by truncating the infrared part of the spectrum. These instabilities are only tamed by multi-angle effects.

VI. MULTI-ANGLE STABILITY ANALYSIS

A. The consistency conditions

The linearized stability analysis in the single-angle case shed new light on the self-consistency conditions as originating from a simple eigenvalue equation, although the conditions themselves had been found previously together with the full solution independently of the small-amplitude expansion. However, the single-angle approximation is not justified in the SN context except that numerically single-angle simulations and multi-angle simulation sometimes, but not always, yield similar results. Therefore, based on the eigenvalue equation (33), we now extend the linearized analysis to the multi-angle case. Besides the small-amplitude expansion, this equation also uses the large-distance approximation where it is assumed that the angular divergence of the neutrino radiation is small.

The crucial step is to realize that the r.h.s. of Eq. (33) is of the form $A + Bu$ where A and B are expressions that do not depend on either ω or u . So we are led to

the ansatz for the form of the eigenfunction

$$Q_{\omega,u} = \frac{a + bu}{\omega + u\bar{\lambda} - \Omega}, \quad (63)$$

where a and b are complex numbers. Inserting this ansatz provides

$$a + bu = \mu \int du' d\omega' g_{\omega',u'} \frac{(u + u')(a + bu')}{\omega' + u'\bar{\lambda} - \Omega}. \quad (64)$$

To understand better the structure of this equation, we define the integrals

$$I_n = \int du d\omega g_{\omega,u} \frac{u^n}{\omega + u\bar{\lambda} - \Omega}. \quad (65)$$

Then our eigenvalue equation becomes

$$a + bu = \mu \left[(aI_1 + bI_2) + (aI_0 + bI_1)u \right]. \quad (66)$$

If this is supposed to be true for every u we need to match the coefficients of the linear u polynomial on both sides separately. We can then write this in matrix form

$$\mu^{-1} \begin{pmatrix} a \\ b \end{pmatrix} = \begin{pmatrix} I_1 & I_2 \\ I_0 & I_1 \end{pmatrix} \begin{pmatrix} a \\ b \end{pmatrix}. \quad (67)$$

This has the form of an eigenvalue equation for a 2×2 matrix. This equation has nontrivial solutions if

$$\det \left[\begin{pmatrix} I_1 & I_2 \\ I_0 & I_1 \end{pmatrix} - \mu^{-1} \right] = 0 \quad (68)$$

or explicitly

$$\mu^{-1} = I_1 \pm \sqrt{I_0 I_2}. \quad (69)$$

This is the multi-angle counterpart of our single-angle eigenvalue equation of Eq. (37).

We introduce once more $\Omega = \gamma + i\kappa$, and to split this equation into its real and imaginary parts we write the integral expressions in the form

$$I_n = J_n + iK_n, \quad (70)$$

where

$$J_n = \int d\omega du g_{\omega,u} u^n \frac{\omega + u\bar{\lambda} - \gamma}{(\omega + u\bar{\lambda} - \gamma)^2 + \kappa^2},$$

$$K_n = \int d\omega du g_{\omega,u} u^n \frac{\kappa}{(\omega + u\bar{\lambda} - \gamma)^2 + \kappa^2}. \quad (71)$$

Inserting this into Eq. (69) and equating the real and imaginary parts separately yields the two real equations

$$(J_1 - \mu^{-1})^2 = K_1^2 + J_0 J_2 - K_0 K_2,$$

$$(J_1 - \mu^{-1}) = \frac{J_0 K_2 + K_0 J_2}{2K_1}. \quad (72)$$

These two equations can now be taken as our consistency conditions, analogous to Eqs. (38) and (39) in the single-angle case.

Note that for a given angular mode $u = u_0$, the quantity $|Q_{\omega,u_0}|^2$ is a Lorentzian, centered at $\omega = \gamma - u_0\bar{\lambda}$. Thus, the range of ω -modes that are affected by the instability is different for different angular modes, as opposed to the single-angle case.

In order to solve for γ and κ satisfying the consistency conditions, one may consider μ and $\bar{\lambda}$ as independent quantities, keeping in mind the constraint $\lambda = \bar{\lambda} - \epsilon\mu$. This allows us to find one real equation from which μ is eliminated. As in the single-angle case, this equation provides a μ -independent relation between γ and κ and thus the set of all possible eigenvalues. The set of all points in the $\Omega = \gamma + i\kappa$ plane fulfilling this requirement represents the ‘‘root locus diagram’’ of our self-consistency relations. The other equation is of the form $\mu^{-1} = (\text{integral expressions})$ and allows one to calculate for any allowed $\Omega = \gamma + i\kappa$ the corresponding μ by quadratures alone.

The energy and angular distributions of SN neutrinos are not independent of each other. On the other hand, in schematic models one may assume that the angular distribution is independent of energy and independent of flavor. In particular, the approximation of a common blackbody neutrino sphere for all flavors implies $g_{\omega,u} = g_{\omega}$, independently of u . In this case the u integration in the expressions for I_n can be performed explicitly, considerably simplifying the numerical inversion of the self-consistency equations.

B. Matter vs. neutrino background

Multi-angle effects on the stability of the spectrum may be interpreted in terms of the separate effects of the two terms on the r.h.s. of the EoM in Eq. (31). The second term represents the effects of Pantaleone’s off-diagonal refractive index caused by neutrino-neutrino interactions. It allows for the instability in the first place and in addition can lead to self-induced multi-angle decoherence [26, 27]. However, this decoherence effect arises after some pendular oscillations and would not be visible in the small-amplitude expansion. Decoherence arises in a periodic system performing many revolutions and different modes dephasing relative to each other. The unstable solution in the small-amplitude expansion is not periodic, but exponentially growing, and thus we can not study decoherence effects. However, we can study the multi-angle modification of the instability which is caused by $\bar{\lambda}$ in the first term on the r.h.s. of Eq. (31).

If Pantaleone’s flavor off-diagonal refractive effect would not exist, i.e. the last term on the r.h.s. in Eq. (31) would be missing, then the first term on the r.h.s. specifies that every mode $S_{\omega,u}$ freely precesses around the weak-interaction direction with frequency $\omega_{\text{eff}} = \omega + (\lambda + \epsilon\mu)u$. We recall that

$$\lambda = \sqrt{2}G_{\text{F}}(n_e - n_{\bar{e}}) \frac{R^2}{2r^2}, \quad (73)$$

as given in Eq. (21), represents the net matter effect in the co-rotating frame. Note that we have kept only the matter term causing an angle-dependent spread of ω_{eff} , while the main matter effect, causing a common precession with frequency $\sqrt{2}G_{\text{F}}(n_e - n_{\bar{e}})$, has been removed by going to a rotating frame.

The flavor-diagonal refractive effect caused by the neutrino background, in our equations represented by $\epsilon\mu$, plays a perfectly analogous role to ordinary matter. Indeed, it is the quantity $\bar{\lambda} = \lambda + \epsilon\mu$ which appears in the EoMs, and hence in the multi-angle analysis. Though we define the neutrino background contribution in terms of the radial flux densities and not their number densities, at large distances these two quantities are identical. Therefore, we may write

$$\epsilon\mu = \sqrt{2}G_{\text{F}}[(n_{\nu_e} - n_{\bar{\nu}_e}) - (n_{\nu_x} - n_{\bar{\nu}_x})] \frac{R^2}{2r^2}. \quad (74)$$

The matter background term λ and the neutrino background term $\epsilon\mu$ are completely symmetric, if one takes into account that the x contribution is missing among charged leptons simply because of the absence of charged x leptons since both μ and τ leptons are too heavy to be present in the SN context.

C. Multi-angle suppression of the instability

A large matter effect in the form of a large value of $\bar{\lambda} = \lambda + \epsilon\mu$ can suppress the self-induced instability in numerical SN simulations. This effect was predicted in Ref. [30] and has been repeatedly tested, most recently in the numerical studies of Ref. [24]. The reason invoked for this suppression was the large dispersion of $\omega_{\text{eff}} = \omega + \bar{\lambda}u$ that is caused if u is spread over the unit interval and $\bar{\lambda}$ is much larger than the direct spectral spread of ω . It was then argued that this multi-angle matter suppression of the instability would be noticeable if the matter term were much larger than the neutrino background term, i.e. if $\lambda \gg \mu$. The linearized analysis allows us to show analytically that when $\bar{\lambda} \gg \mu$, the collective oscillations are completely suppressed.

Let ω_{max} be the largest value of $|\omega|$ where $g_{\omega,u}$ is significant. When $\bar{\lambda} \gg \omega_{\text{max}}$, the quantities I_n in Eq. (65) are suppressed due to the factor of $\bar{\lambda}u$ in the denominator. The cancellation of large values of $\bar{\lambda}u$ by Ω is possible only in a narrow range of u values, which will give only a small contribution to the integral. Equation (69) can then be satisfied only at $\mu \sim \bar{\lambda}$. Therefore, the system should be stable for $\bar{\lambda} \gg \mu$, i.e. when the net effects of ordinary matter dominate over those of the neutrino-neutrino interactions.

A seemingly different multi-angle suppression affects the ‘‘saturation mode’’ of collective oscillations that can occur in spectra with at least two zero crossings for very large μ (Secs. IV B and IV C). This mode was first discovered in an analytic toy model [28] and later re-discovered

in the context of a more realistic SN example [29]. Moreover, both papers argued and tested numerically that the spread of ω_{eff} caused by the neutrino-neutrino term would suppress the saturation mode. This suppression effect, however, is just another aspect of the impact of $\bar{\lambda}$ in the EoMs. The matter and neutrino backgrounds together cause a common multi-angle effect by dispersing ω_{eff} . This may be seen as follows.

In the single-angle approach and for spectra with ϵ not very small, the consistency relations imply that κ cannot be much larger than a typical spread $\Delta\omega$ of the frequency spectrum. Indeed, for $\kappa \gg \Delta\omega$, Eq. (38) would not be satisfied for any finite asymmetry ϵ . Assuming that κ and thus the resonance width remains of order $\Delta\omega$ in the multi-angle case, it is clear that a large dispersion of ω_{eff} shifts most modes away from the resonance. In this way, multi-angle effects would indeed suppress self-induced flavor conversions at large $\bar{\lambda}$. We will see that the presence of a large $\bar{\lambda}$ in the EoMs will never increase κ significantly, although it can suppress it considerably. In this sense the reasons given here for the multi-angle matter suppression indeed apply.

For certain spectra, notably the generic two-box case, the single-angle approximation predicts a cutoff μ_{sync} . The instability cannot form at large values of μ since the consistency conditions in Eqs. (38) and (39) cannot be satisfied for any complex Ω , and the system is stable. For $\mu < \mu_{\text{sync}}$, however, pendular oscillations commence. The multi-angle analysis does not change this behavior qualitatively. The value of μ_{sync} in the multi-angle case is some average of the μ_{sync} values for different u_0 values, as can be seen in Fig. 2.

D. Normal vs. inverted mass hierarchy

In the single-angle approximation, we saw that as far as the stability analysis is concerned, analysis of normal hierarchy is the same as that of the inverted one, except for a change of the sign of μ . This is true also in the multi-angle scenario, except that one also needs to change the sign of λ . Indeed, normal hierarchy changes Eq. (31) to

$$\begin{aligned} i\partial_r \tilde{S}_{\omega,u} &= [-\omega + u(\lambda + \epsilon\mu)] \tilde{S}_{\omega,u} \\ &\quad - \mu \int du' d\omega' (u + u') g_{\omega'u'} \tilde{S}_{\omega',u'}. \end{aligned} \quad (75)$$

The solution of this equation can be given in terms of the solution $S_{\omega,u}$ of Eq. (31) as

$$\begin{aligned} \tilde{S}_{\omega,u}(\mu, \lambda, g_{\omega,u}) &= S_{\omega,u}^*(\mu, -\lambda, -g_{\omega,u}) \\ &= S_{\omega,u}^*(-\mu, -\lambda, g_{\omega,u}). \end{aligned} \quad (76)$$

Since S and S^* should have the same stability behavior, this implies that the stability conditions for normal hierarchy are the same as those for the inverted hierarchy with a change in the sign of g_{ω} or μ (not both at the same time), and an additional change in the sign of λ .

VII. MULTI-ANGLE EXAMPLES

We now study the stability conditions including multi-angle effects for the box spectra considered earlier as well as for a realistic SN example. It turns out that the multi-angle effects modify the single-angle results in significant ways. We always take the emission to be uniform over $0 \leq u \leq 1$. The integrals J_n and K_n can then be analytically calculated for the box spectra. The expressions, however, are not very illuminating, and we do not give them here.

A. Two boxes

The two-box spectrum and the single-angle eigenvalues $\gamma(\mu)$ and $\kappa(\mu)$ for different choices of the emission angle u_0 were shown in Fig. 2. In addition, we show in Fig. 2 the numerical result for $\gamma(\mu)$ and $\kappa(\mu)$ in the multi-angle case, assuming the absence of matter so that $\bar{\lambda} = \epsilon\mu$ and all effects are caused by neutrino-neutrino interactions alone. As far as the stability behavior is concerned, the multi-angle effects may be interpreted as some (complicated) average of the single-angle effects with different u_0 values. In particular, the value of κ at any value of μ lies within the range of κ for different u_0 values in the single-angle approximation. In other words, multi-angle effects leave the system qualitatively unchanged.

For sufficiently dense matter the picture changes considerably. In Fig. 6 we repeat the single-angle results for $u_0 = 1/2$ (thin black dot-dashed curves) and the no-matter multi-angle results (red solid curve). We also show curves for $\lambda = 5$ and 30. Qualitatively the $\gamma(\mu)$ and $\kappa(\mu)$ curves are shifted to larger values of μ , the spectra being stable below some threshold value and above some cutoff value. The interval of unstable μ values remains roughly the same, except that it is shifted to larger μ values. The shift is approximately such that the unstable domain arises for $\mu \sim \bar{\lambda}$ as predicted earlier.

The presence of matter alone does not stabilize the system, it shifts the instability domain to larger μ values. Indeed, a nonzero λ can allow for an instability even at the values of μ where $\epsilon\mu$ alone could not have generated an instability. In the μ - λ plane, the system is unstable along a strip roughly following $\lambda \sim \mu$, and stable outside. In a SN we sweep from large to small μ values as a function of radius, and at the same time from large to small λ values. If everywhere along the path $\lambda \gg \mu$, we would be outside the instability strip.

However, even if this is not the case, the system could still be stabilized. We also have the effect of dispersing the spectrum relative to the resonance condition. In a spectrum of given spectral width $\Delta\omega$, the resonance denominator $\omega + u\bar{\lambda} - \Omega$ will be on resonance only for a narrow range of u values if $\bar{\lambda}$ is large. Therefore, even if the system is not stable, most modes will be off-resonance in analogy to our discussion of spectral tails.

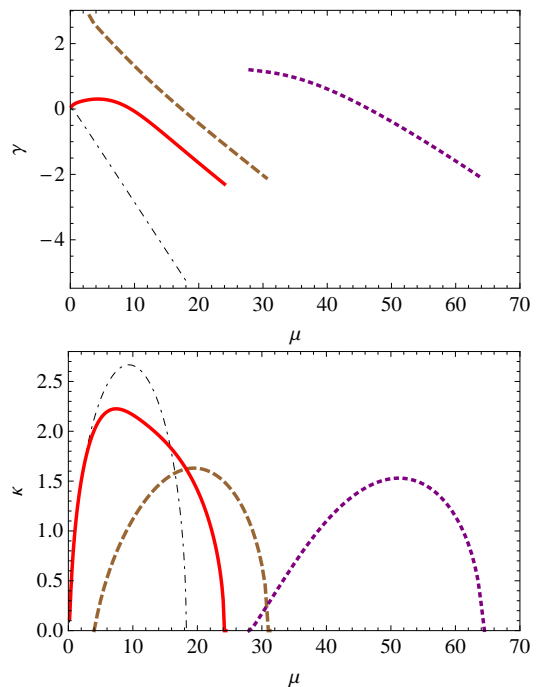


FIG. 6: Multi-angle eigenvalues $\gamma(\mu)$ and $\kappa(\mu)$ for the two-box spectrum in Fig. 2. Black (dash-dotted) thin line: single-angle ($u_0 = 1/2$). All other lines: multi-angle. Red (solid): no matter ($\lambda = 0$). Brown (dashed): $\lambda = 5$. Purple (dotted): $\lambda = 30$. The $\gamma(\mu)$ curves are only shown where $\kappa(\mu) \neq 0$.

A detailed understanding of the multi-angle stabilization of the neutrino flux streaming from a SN core as studied most recently in Ref. [24] requires more detailed scrutiny because the described effects of shift and dispersion both affect a realistic SN neutrino flux.

B. Three boxes

We now turn to the three-box example of Fig. 3 which was chosen such that we observe a “saturation mode:” The system is unstable with an asymptotic value of κ for arbitrarily large μ and the center of the resonance γ remains centrally located in the spectral range. Here the multi-angle matter effect causes a dramatic modification of the single-angle results because the curve $\kappa(\mu)$ is completely suppressed above a critical μ -value, i.e. the spectrum is actually stabilized.

In Fig. 7 we repeat the single-angle case with $u_0 = 1/2$ and show the multi-angle case with vanishing matter so that $\bar{\lambda} = \epsilon\mu$. The previous saturation effect is completely suppressed. As we increase λ , the instability domain is shifted to larger μ values roughly linearly with λ as explained earlier. In other words, the system now behaves similar to the two box case.

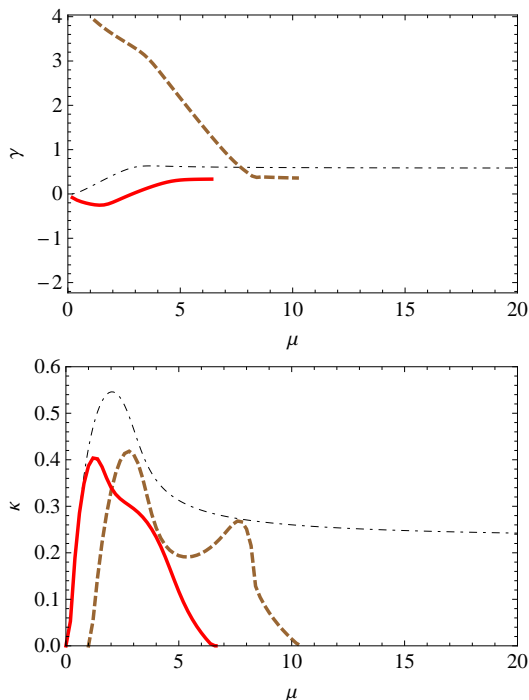


FIG. 7: Multi-angle eigenvalues $\gamma(\mu)$ and $\kappa(\mu)$ for the three-box spectrum in Fig. 3. Black (dash-dotted) thin line: single-angle ($u_0 = 1/2$). All other lines: multi-angle. Red (solid): no matter ($\lambda = 0$). Brown (dashed): $\lambda = 5$. The $\gamma(\mu)$ curves are only shown where $\kappa(\mu) \neq 0$.

C. Four boxes

The main novelty of the four-box spectrum is that it can display two simultaneous instabilities. One of them can be of the saturation type, similar to the three-box example, details depending on the exact choice of parameters. Multi-angle effects for $\lambda = 0$ and thus $\bar{\lambda} = \epsilon\mu$ are shown in Fig. 4. The results are entirely in line with the expectations from the previous examples in that the saturation mode gets suppressed at large μ . We shall not repeat the analysis with the four-box spectra here. However the realistic SN spectrum in the next section can be seen to be close to a four-box spectrum, and is observed to display the same expected behavior.

D. A realistic SN spectrum

We now apply our stability analysis to a realistic SN spectrum that is motivated by Duan and Friedland’s recent numerical study of multi-angle suppression [29]. They used ν_e , $\bar{\nu}_e$, and ν_x spectra with assumed Fermi-Dirac form. The temperatures were taken to be 2.1, 3.5, and 4.4 MeV, respectively, and the degeneracy parameters 3.9, 2.3 and 2.1. The average energies are then 9.4, 13.0 and 15.8 MeV. The ratios of number fluxes are taken to be 1.3 : 1.0 : 1.5, where the total $\bar{\nu}_e$ flux is normalized

to unity as per our convention introduced in Sec. II A. We use $\Delta m^2 = (50\text{meV})^2$ in order to convert the energy scale to ω , which we show in the units of km^{-1} .

The spectrum is shown in the top panel of Fig. 8. It has three spectral crossings and thus compares with a four-box spectrum, although the deviation from zero of the left-most part is almost invisible. (For $\omega < -0.8$, the value of g_ω is small and negative.) The main feature of interest here and in Duan and Friedland’s study is the presence of a “saturation mode” in which the instability in the single-angle treatment exists for arbitrarily large μ . Such a feature requires at least two crossings, so in this regard the visual impression of this being a “three box” example is actually the main point.

In single angle (thin dot-dashed black line) we find a dominant “saturation mode” as expected (corresponding to γ_2, κ_2) and in addition a “cutoff mode” (corresponding to γ_1, κ_1) which always has very small values for $\kappa(\mu)$. The existence of this mode is a residue of the not perfect disappearance of g_ω at $\omega \lesssim -0.8$, i.e. of the small “fourth box.” If we were to truncate the spectrum at the left-most crossing, this mode would disappear. At very small μ , these two instabilities are centered near the positive spectral crossings as expected. Even the “cutoff mode” does not completely disappear for large μ due to the spectral tails.

Next we include multi-angle effects without matter ($\lambda = 0$), roughly corresponding to the study of Ref. [29] where the matter density was small compared to the neutrino density. The red solid curve represents the case with $\bar{\lambda} = \epsilon\mu$. We see that at large μ , corresponding to small radii in the SN, the saturation mode is indeed suppressed. It does not vanish completely, owing to the presence of spectral tails, in contrast to the earlier box examples. The center of the saturation mode, $\gamma_2 - u\epsilon\mu$, continues to be in the central part of the spectrum for $u \approx 1$. The center of the cut-off mode, $\gamma_1 - u\epsilon\mu$, on the other hand, is actually pushed into the tail of the spectrum.

Next we add a significant amount of matter, represented by $\lambda = 5$ (brown dashed curves). There now a lower μ -threshold appears for both, the cutoff mode as well as the saturation mode. This is a consequence of the complete suppression of collective oscillations at $\bar{\lambda} \gg \mu$, predicted in Sec. VI C. Thus, our analytical prediction is vindicated in this scenario of a realistic SN spectrum.

The main result of Ref. [29], obtained in the regime $\bar{\lambda} \sim \mu$, was that multi-angle effects stabilize the spectrum in deep layers of the SN where in single-angle strong bipolar oscillations would have occurred. Our stability analysis provides two reasons for this behavior. The value of $\kappa(\mu)$ is strongly reduced, although the spectrum is always unstable as behooves a spectrum with tails. Moreover, the dispersion of effective oscillation frequencies due to the presence of $u\bar{\lambda}$ in the resonance denominator moves most modes off resonance. Given $\mu(r)$ and $\lambda(r)$, one can predict the exact SN radius where serious bipolar oscillations would kick in for the multi-angle case, with the stability analysis.

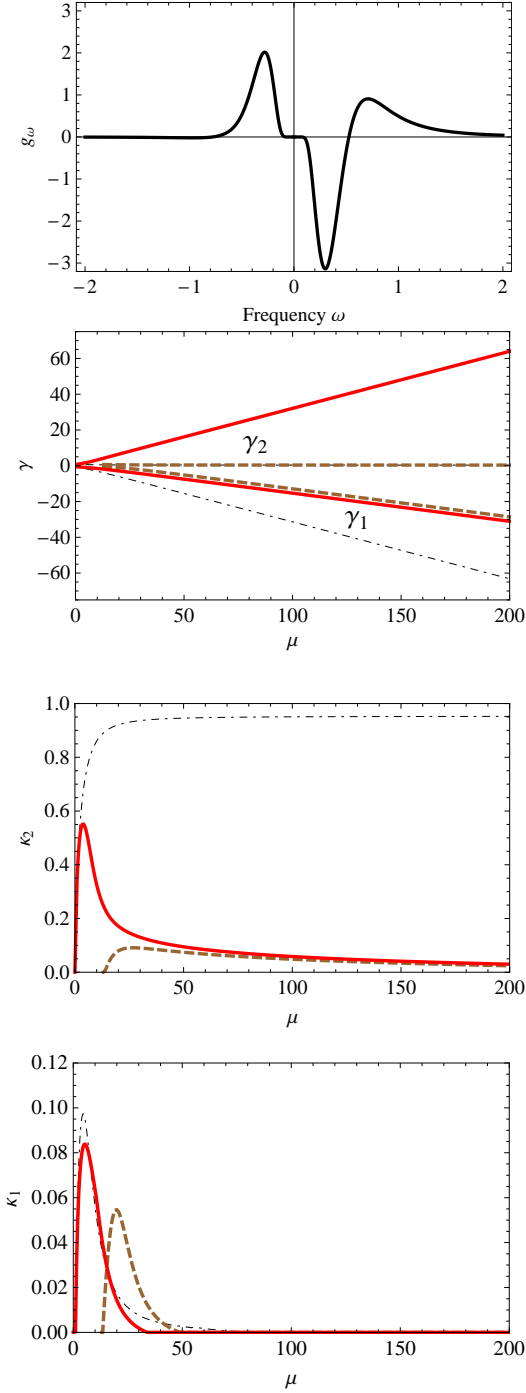


FIG. 8: Realistic SN spectrum as described in the text and identical with Ref. [29]. Lower panels: $\gamma(\mu)$ and $\kappa(\mu)$ for the two instabilities, where 1 denotes the one with smaller γ . Mode 2 is the saturation mode. Black (dash-dotted) thin line: single-angle ($u_0 = 1/2$), otherwise multi angle. Red (solid): no matter ($\lambda = 0$). Brown (dashed): $\lambda = 5$.

VIII. MULTI-ANGLE INSTABILITY IN NORMAL HIERARCHY

A perfectly symmetric spectrum shows self-induced kinematical decoherence among angular modes in either hierarchy, or in the language of our present study, whether the zero-crossing of g_ω is positive or negative [26]. The same is found for spectra with a small asymmetry $\epsilon \ll 1$ [27]. Kinematical decoherence requires the spectrum to be unstable in the first place, so these findings imply that in the multi-angle case, an instability does not require a positive zero-crossing of g_ω . This surprising result is easily verified with our method.

Let us assume that $\lambda = 0$, as would be the case for an antisymmetric spectrum ($\epsilon = 0$) and in the absence of matter. We further make the simplifying assumption of a universal angular distribution, i.e. $g_{\omega,u} = g_\omega f_u$, with $\int du f_u = 1$. Let us introduce the notation

$$G = \int d\omega \frac{g_\omega}{\omega - \Omega}. \quad (77)$$

Then in the multi-angle case, we have

$$I_n = G \int_0^1 du u^n = G \langle u^n \rangle. \quad (78)$$

The eigenvalue equation is then

$$\mu^{-1} = I_1 \pm \sqrt{I_0 I_2} = [\langle u \rangle \pm \langle u^2 \rangle^{1/2}] G. \quad (79)$$

The stability analysis then corresponds to determining the solutions $\Omega = \gamma \pm i\kappa$ for the equation

$$\mu^{-1} = \mathcal{K}_\pm G, \quad (80)$$

where $\mathcal{K}_\pm \equiv \langle u \rangle \pm \langle u^2 \rangle^{1/2}$.

In the single-angle approximation, $\langle u \rangle = u_0$, $\langle u^2 \rangle = u_0^2$, so that $\mathcal{K}_+ = 2u_0$ and $\mathcal{K}_- = 0$. The latter equation has no solution, since it would require $\mu^{-1} = 0$ identically. One may then write

$$\mu_{\text{single}}^{-1} = 2u_0 G. \quad (81)$$

This may be solved to obtain the values of γ and κ in the single-angle approximation. Clearly, μ_{single}^{-1} has the same sign as G , so that G is positive for a spectrum with positive crossing.

We can now write the two values of μ^{-1} in multi-angle analysis that correspond to the same values of γ and κ :

$$\mu_+^{-1} = \mathcal{K}_+ G, \quad \mu_-^{-1} = \mathcal{K}_- G, \quad (82)$$

Thus, there are two values of μ in multi-angle analysis that correspond to the same (γ, κ) in the single-angle analysis. The multi-angle stability behavior at these two μ values can then be understood in terms of the single-angle stability behavior at μ_{single} .

Note that $\mathcal{K}_+ \geq 0$ and $\mathcal{K}_- \leq 0$. Therefore, μ_+ is positive, and it corresponds to just a scaled value of

μ_{single} with the same (inverted) hierarchy. The single-angle study is indeed a good proxy for the multi-angle case in such a scenario. On the other hand, μ_- is negative, and corresponds to the normal hierarchy. For spectra with $\langle u^2 \rangle^{1/2} \sim \langle u \rangle$ one finds that $|\mu_-| \gg |\mu_+|$, so the “wrong hierarchy” case shows the same instability at much larger densities.

The exact mapping between the single- and multi-angle cases is not possible for the more realistic case of $\bar{\lambda}$ being small but nonzero, but of course we expect a qualitatively similar behavior.

In Ref. [27] it was found that kinematical decoherence is suppressed for sufficiently large ϵ , which in normal hierarchy means that the spectrum is stable and the “positive crossing” rule for an instability is back in force. These studies did not include the presence of matter, so $\bar{\lambda} = \epsilon\mu$ with a sufficiently large ϵ implied that $\bar{\lambda}$ was not very small. In this sense, the stability in normal hierarchy for sufficiently large ϵ looks like yet another case of multi-angle suppression of an instability.

IX. CONCLUSIONS AND OUTLOOK

The refractive effect of neutrino-neutrino interactions can cause a flavor instability among the different energy and angular modes, exchanging the flavor content while leaving unchanged the overall flavor content of the entire ensemble. In the context of SN neutrinos, the focus so far has been on impacts of collective flavor oscillations on the neutrino signal of the next nearby SN or for the r-process nucleosynthesis. Many analyses have been performed under the simplifying assumption that all neutrinos feel the same refractive effect due to the other neutrinos (single-angle assumption). However it has also been found that multi-angle effects can strongly modify the answer and can typically suppress flavor conversions that would occur in the single-angle treatment. In this sense, a more pressing question is to understand the stability conditions for a dense neutrino stream, and to understand if the usual neglect of flavor oscillations in those dense SN regions is justified where a Boltzmann treatment of neutrino transport is necessary.

We have studied the conditions under which instabilities can occur in the neutrino stream in the two-flavor framework. While the equations of motion are nonlinear, the run-away solutions can be found by a standard mode analysis of the linearized system, i.e. in the small-amplitude expansion. We have shown how the stability question is reduced to a straightforward eigenvalue equation in the co-rotating frame. The existence of complex eigenvalues directly corresponds to an instability. In the multi-angle case, besides the small-amplitude expansion, we have linearized the equations in the small angular divergence of the neutrino flux that is applicable at a large distance from the source. In the single-angle case, our conditions agree with the previous literature, whereas in the multi-angle case, our results are new.

In the single-angle case and using schematic energy spectra (box spectra in the ω variable), the eigenvalue equation can be solved analytically. We identify two generic instability cases. The “cutoff mode” exists for a finite range of neutrino densities, or equivalently, a finite interval of effective neutrino-neutrino interaction strengths $\mu_0 < \mu < \mu_1$. In particular, the system is stable above a cutoff value μ_1 , also termed the “synchronization” or “sleeping top” regime. This behavior is generic to a single-crossed (or two-box) spectrum and represents the traditional flavor pendulum. On the other hand, there is the “saturation mode” where the instability approaches an asymptotic value for large μ . This mode requires at least two crossings (three boxes) and had been previously found in the literature. When it exists, the saturation mode exists for both hierarchies. For multi-crossed spectra, several modes can co-exist, for example in the four-box case a saturation mode and a cutoff mode or two cutoff modes.

An additional case occurs for neutrino spectra with a vanishing asymmetry, i.e. with no net lepton number flux. The run-away rate κ grows indefinitely as a function of μ . This actually is a special case of the cutoff mode (cutoff at infinite μ) and does not seem to be of practical interest in the SN context.

Realistic neutrino spectra are not described by boxes and have tails as a function of $\omega = |\Delta m^2|/2E$, corresponding to infrared energies. Such spectra do not have a cutoff and a synchronization regime does not exist. However, for large μ the instability moves entirely into the infrared regime and has no practical impact. There remains an effective cutoff density where the amount of flavor exchange between modes drops by orders of magnitude within a narrow range of neutrino densities. Still, the existence of a synchronization regime is only an approximate concept.

Multi-angle effects modify the instability in several ways. For example, while the single-angle approximation predicts an instability only if there is a positive zero-crossing of the spectrum g_ω , the multi-angle analysis implies that spectra with a small asymmetry (a small net lepton number flux) and in the absence of matter are unstable in both hierarchies, whatever be the sign of the zero-crossing. The solutions for both hierarchies can be mapped onto each other.

The main multi-angle modification of the instability is caused by a background of matter, where here neutrinos themselves also contribute to the matter effect. The saturation mode is “fragile” and, for box spectra, develops a cutoff. (For realistic spectra with tails, there is no exact cutoff, however, as mentioned earlier.) The neutrino background alone is enough to achieve this effect.

For both the saturation and cutoff modes, a large matter effect shifts the domain of instability $\mu_0 < \mu < \mu_1$ to larger values of μ . The amount of shift is approximately equal to the matter potential λ , apparently without reducing the typical κ values within the instability domain. An additional consequence is that the affected range of

modes shrinks for increasing λ . Even if the run-away scale κ is not reduced, only a narrow range of angular modes is on resonance if λ is large. For realistic spectra with tails, $\kappa(\mu)$ does not vanish for large μ , i.e. there is not an exact cutoff. On the other hand, there is a lower threshold $\mu_0 \sim \lambda$ below which the spectrum is completely stable. In other words, multi-angle effects introduce a range $0 < \mu < \mu_0 \sim \lambda$ where the spectrum is stable even when such a stable range does not exist in the single-angle approximation. This behavior corresponds to the multi-angle suppression of instability at $\lambda \gg \mu$, which we motivate analytically through our linearized treatment.

One may further investigate these findings in the context of realistic SN situations where neutrinos stream from regions of large density to vacuum, sweeping through μ values from very large to zero. The central frequency γ of the instability then sweeps through different spectral ranges and the growth rate κ depends on both the neutrino and matter density. Effective flavor conversion can be suppressed in different ways: The growth rate κ can vanish when μ falls into the multi-angle-implied stability domain, or it can be too small on the available distance scale, or the instability can be located mostly in the infrared and affect only an ignorable part of the spectrum.

We have considered neutrinos streaming from a source and have made the approximation of small angular divergence that is appropriate at a large distance from the source. Our approach can be easily adapted to a homogeneous ensemble with a nontrivial angular distribution that evolves in time rather than as a function of distance from a source. In this case no expansion in the angular variable is needed.

We have only considered trivial angular distributions where all neutrino flavors are assumed to be emitted from a common blackbody sphere without limb darkening, cor-

responding to a box spectrum in our u variable. One can extend our analysis to more complicated angular distributions that could involve, for example, spectral crossings in the angular variable. As advocated by Sawyer, such crossings cause a “multi-angle instability,” but its practical relevance remains to be investigated.

We have made the usual assumption of azimuthal symmetry of the neutrino flux around the radial direction away from the source. In the long-distance limit of small angular divergence of the neutrino field, one can of course expand the EoMs in terms of small variables that depend on two angles. It remains to be explored if cylindrical symmetry enforces unphysical solutions, just as the single-angle approximation sometimes enforces unphysical solutions, and if there are new instabilities or important modifications that could be relevant in the SN context. Based on schematic models using a small number of modes it has been suggested that violations of cylindrical symmetry could have a major impact [13].

A rich phenomenology of neutrino flavor conversions is bound to emerge from further investigations into the collective effects due to neutrino-neutrino interactions and ordinary matter background, in the complete multi-angle framework.

Acknowledgements

We would like to thank Basudeb Dasgupta, Srdjan Sarikas and Ray Sawyer for their comments on the manuscript. In Munich, this work was partly supported by the Deutsche Forschungsgemeinschaft under grants TR-27 and EXC-153. G.R. thanks the Tata Institute of Fundamental Research (Mumbai) for hospitality while this work was begun.

-
- [1] L. Wolfenstein, “Neutrino oscillations in matter,” *Phys. Rev. D* **17**, 2369 (1978).
 - [2] S. P. Mikheev and A. Y. Smirnov, “Resonance enhancement of oscillations in matter and solar neutrino spectroscopy,” *Sov. J. Nucl. Phys.* **42**, 913 (1985) [*Yad. Fiz.* **42**, 1441 (1985)].
 - [3] S. P. Mikheev and A. Y. Smirnov, “Neutrino oscillations in a variable density medium and neutrino bursts due to the gravitational collapse of stars,” *Sov. Phys. JETP* **64**, 4 (1986) [*Zh. Eksp. Teor. Fiz.* **91**, 7 (1986)] [arXiv:0706.0454].
 - [4] A. S. Dighe and A. Y. Smirnov, “Identifying the neutrino mass spectrum from the neutrino burst from a supernova,” *Phys. Rev. D* **62**, 033007 (2000) [hep-ph/9907423].
 - [5] T. K. Kuo and J. T. Pantaleone, “Neutrino oscillations in matter,” *Rev. Mod. Phys.* **61**, 937 (1989).
 - [6] J. Pantaleone, “Neutrino oscillations at high densities,” *Phys. Lett. B* **287**, 128 (1992).
 - [7] G. Sigl and G. Raffelt, “General kinetic description of relativistic mixed neutrinos,” *Nucl. Phys. B* **406**, 423 (1993).
 - [8] S. Samuel, “Neutrino oscillations in dense neutrino gases,” *Phys. Rev. D* **48**, 1462 (1993).
 - [9] V. A. Kostelecký and S. Samuel, “Neutrino oscillations in the early universe with an inverted neutrino mass hierarchy,” *Phys. Lett. B* **318**, 127 (1993).
 - [10] V. A. Kostelecký and S. Samuel, “Self-maintained coherent oscillations in dense neutrino gases,” *Phys. Rev. D* **52**, 621 (1995). [hep-ph/9506262].
 - [11] S. Samuel, “Bimodal coherence in dense selfinteracting neutrino gases,” *Phys. Rev. D* **53**, 5382 (1996). [hep-ph/9604341].
 - [12] R. F. Sawyer, “Speed-up of neutrino transformations in a supernova environment,” *Phys. Rev. D* **72**, 045003 (2005) [hep-ph/0503013].
 - [13] R. F. Sawyer, “The multi-angle instability in dense neutrino systems,” *Phys. Rev. D* **79**, 105003 (2009) [arXiv:0803.4319].
 - [14] H. Duan, G. M. Fuller, J. Carlson and Y. Z. Qian, “Simulation of coherent non-linear neutrino flavor trans-

- formation in the supernova environment. I: Correlated neutrino trajectories,” *Phys. Rev. D* **74**, 105014 (2006) [astro-ph/0606616].
- [15] G. Raffelt and A. Yu. Smirnov, “Self-induced spectral splits in supernova neutrino fluxes,” *Phys. Rev. D* **76**, 081301 (2007); Erratum *ibid.* **77**, 029903 (2008) [arXiv:0705.1830]; “Adiabaticity and spectral splits in collective neutrino transformations,” *Phys. Rev. D* **76**, 125008 (2007) [arXiv:0709.4641].
- [16] H. Duan, G. M. Fuller and Y. Z. Qian, “A simple picture for neutrino flavor transformation in supernovae,” *Phys. Rev. D* **76**, 085013 (2007) [arXiv:0706.4293].
- [17] G. L. Fogli, E. Lisi, A. Marrone and A. Mirizzi, “Collective neutrino flavor transitions in supernovae and the role of trajectory averaging,” *JCAP* **0712**, 010 (2007) [arXiv:0707.1998].
- [18] G. L. Fogli, E. Lisi, A. Marrone, A. Mirizzi and I. Tamborra, “Low-energy spectral features of supernova (anti)neutrinos in inverted hierarchy,” *Phys. Rev. D* **78**, 097301 (2008) [arXiv:0808.0807].
- [19] B. Dasgupta, A. Dighe, G. Raffelt and A. Yu. Smirnov, “Multiple spectral splits of supernova neutrinos,” *Phys. Rev. Lett.* **103**, 051105 (2009) [arXiv:0904.3542].
- [20] H. Duan, G. M. Fuller and Y. Z. Qian, “Collective neutrino oscillations,” *Annu. Rev. Nucl. Part. Sci.* **60**, 569 (2010).
- [21] S. Hannestad, G. Raffelt, G. Sigl and Y. Y. Y. Wong, “Self-induced conversion in dense neutrino gases: Pendulum in flavor space,” *Phys. Rev. D* **74**, 105010 (2006); Erratum *ibid.* **76**, 029901 (2007) [astro-ph/0608695].
- [22] H. Duan, G. M. Fuller, J. Carlson and Y. Z. Qian, “Analysis of collective neutrino flavor transformation in supernovae,” *Phys. Rev. D* **75**, 125005 (2007) [astro-ph/0703776].
- [23] G. G. Raffelt, “N-mode coherence in collective neutrino oscillations,” *Phys. Rev. D* **83**, 105022 (2011) [arXiv:1103.2891].
- [24] S. Chakraborty, T. Fischer, A. Mirizzi, N. Saviano and R. Tomàs, “Analysis of matter suppression in collective neutrino oscillations during the supernova accretion phase,” arXiv:1105.1130.
- [25] B. Dasgupta, E. P. O’Connor and C. D. Ott, “The role of collective neutrino flavor oscillations in core-collapse supernova shock revival,” arXiv:1106.1167.
- [26] G. G. Raffelt and G. Sigl, “Self-induced decoherence in dense neutrino gases,” *Phys. Rev. D* **75**, 083002 (2007) [hep-ph/0701182].
- [27] A. Esteban-Pretel, S. Pastor, R. Tomàs, G. G. Raffelt and G. Sigl, “Decoherence in supernova neutrino transformations suppressed by deleptonization,” *Phys. Rev. D* **76**, 125018 (2007) [arXiv:0706.2498].
- [28] G. G. Raffelt, “Self-induced parametric resonance in collective neutrino oscillations,” *Phys. Rev. D* **78**, 125015 (2008) [arXiv:0810.1407].
- [29] H. Duan and A. Friedland, “Self-induced suppression of collective neutrino oscillations in a supernova,” *Phys. Rev. Lett.* **106**, 091101 (2011) [arXiv:1006.2359].
- [30] A. Esteban-Pretel, A. Mirizzi, S. Pastor, R. Tomàs, G. G. Raffelt, P. D. Serpico and G. Sigl, “Role of dense matter in collective supernova neutrino transformations,” *Phys. Rev. D* **78**, 085012 (2008) [arXiv:0807.0659].
- [31] A. D. Dolgov, “Neutrinos in the early universe,” *Sov. J. Nucl. Phys.* **33**, 700 (1981) [*Yad. Fiz.* **33**, 1309 (1981)].
- [32] Y. Pehlivan, A. B. Balantekin, T. Kajino and T. Yoshida, “Invariants of collective neutrino oscillations,” arXiv:1105.1182.
- [33] E. A. Yuzbashyan, “Normal and anomalous solitons in the theory of dynamical Cooper pairing,” *Phys. Rev. B* **78**, 184507 (2008)